

Independent excitations of the spin and orbital momenta in a single magnetic atom

R. Rejali,^{1,*} D. Coffey,¹ J. Gobeil,¹ J. W. González,² F. Delgado,³ and A. F. Otte^{1,†}

¹*Department of Quantum Nanoscience, Kavli Institute of Nanoscience, Delft University of Technology, Lorentzweg 1, 2628 CJ Delft, The Netherlands.*

²*Departamento de Física, Universidad Técnica Federico Santa María, Casilla Postal 110V, Valparaíso, Chile.*

³*Departamento de Física & Instituto de Estudios Avanzados (IUdEA), Universidad de La Laguna, 38200, San Cristóbal de La Laguna, Santa Cruz de Tenerife, Spain*

(Dated: March 21, 2022)

We use spin-polarized inelastic tunneling spectroscopy to probe the magnetic properties of single Fe atoms bound to the nitrogen sites of Cu_2N . We report a zero-field splitting of 18.4 ± 0.1 meV—the largest reported for Fe adatoms on surfaces—which arises from a largely preserved orbital angular momentum. In addition to two distinct inelastic spin excitations, we observe an excitation of the orbital moment, which we describe in terms of a cotunneling mechanism. We explain these observations using density functional theory and multiplet calculations, accounting for the unquenched, anisotropic orbital moment.

Magnetic atoms adsorbed on surfaces are fundamental building blocks for magnetic information processing, with applications in both the classical and quantum domains [1–4]. However, an essential requirement for such applications is a long-lived magnetic state, which is typically limited by thermally induced fluctuations. The energy barrier to flip the magnetic moment is determined by the magnetic anisotropy energy (MAE), which arises from the interplay between the crystal field and spin-orbit coupling. The Coulomb potential generated by the crystal breaks the spherical symmetry of the free atom, thereby lending the orbital moment a certain orientation with respect to the crystallographic axes [5].

The 3d transition elements are of particular interest as, in addition to their natural abundance, they can be easily deposited on surfaces and probed locally by scanning tunneling microscopy (STM) and spectroscopy. Typically, the orbital moment \mathbf{L} is largely quenched due to the crystal field [5, 6]. In the case of an almost fully quenched \mathbf{L} , the spin-orbit coupling only acts to higher order to produce single-site magnetic anisotropy, which leads to MAE values far below the atomic spin-orbit coupling strength. Consequently, the crystal symmetry at the atomic site—and the overlap of the atomic orbitals with the surrounding ligands—plays a crucial role in preserving the orbital angular momentum of the atom.

This effect is illustrated by observations of very large MAE values on adatoms experiencing a nearly axial crystal field. Experiments on Fe and Co atoms bound on the O-sites of $\text{MgO}/\text{Ag}(100)$, which have C_{4v} symmetry, yield zero-field splittings of respectively 14 meV [7] and 58 meV [8]. Co atoms adsorbed atop N on $\text{h-BN}/\text{Ru}(0001)$ display a similarly large MAE of 14 meV [9].

One particularly appealing substrate is the Cu_2N surface [10], where, in addition to the protection of the magnetic moments from electronic scattering provided by the decoupling layer, magnetic adatoms can be easily manipulated [11–16]. STM studies have revealed that Fe

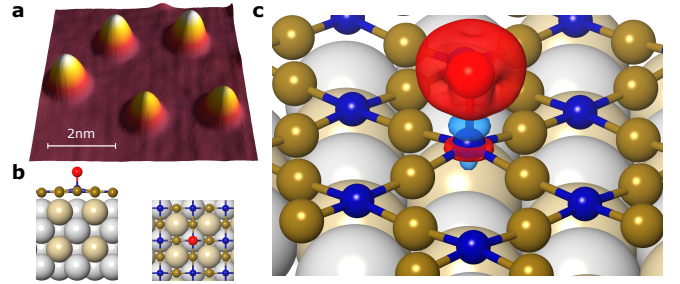


FIG. 1. (a) STM constant-current topography (30 mV, 20 pA) of Fe atoms on a $\text{Cu}_2\text{N}/\text{Cu}_3\text{Au}(100)$ surface. To the bottom right, there are two Fe atoms bound to copper sites, and at the top, three Fe atoms atop nitrogen sites with larger apparent heights. (b) Side (left) and top view (right) of the binding geometry for the Fe atom (red) atop a N atom in the Cu_2N network (Cu brown, N blue) on a Cu_3Au crystal (Cu grey, Au yellow). (c) Calculated positive (red) and negative (blue) electron spin density.

atoms on the Cu_2N lattice preferentially bind to the Cu-site, where the local C_{2v} symmetry produces a partially unquenched orbital moment resulting in in-plane uniaxial magnetic anisotropy energies of ~ 5 meV [12, 15]. In principle, much larger anisotropy values could be expected for Fe atoms bound atop a N-site, owing to the higher C_{4v} symmetry. N-site adsorption on Cu_2N is also preferable over Cu-site adsorption, in that placing an Fe atom on an N-site requires one less atom manipulation procedure [17], vastly improving possibilities for building extended spin arrays. However, previous studies reported that no spin-flip excitations could be resolved for Fe atoms bound to N-sites [10].

Here, by performing inelastic electron tunneling spectroscopy (IETS) with a functionalized tip, we are able to probe well-resolved excitations for N-site Fe atoms. We find that the orbital angular momentum is almost fully preserved in this case, resulting in a zero-field splitting of 18 meV, the largest reported to date for Fe atoms

on surfaces. Moreover, we also observe an excitation at 73 meV, that is interpreted as a full reversal of the orbital moment, while leaving the spin moment unchanged. The results are rationalized in terms of density functional theory (DFT) and electronic multiplet calculations.

Figure 1a shows an STM image of single Fe adatoms deposited on an insulating layer of Cu_2N , grown on a $\text{Cu}_3\text{Au}(100)$ substrate [18]. The apparent height of the Fe atoms atop the N-sites is $\sim 3.1 \text{ \AA}$, roughly 0.4 \AA higher than those on Cu sites. The N binding site is four-fold symmetric (C_{4v}), with four Cu atoms as nearest neighbours, a lateral distance of 1.77 \AA away (Fig. 1b). DFT calculations indicate that the N atom atop which the magnetic atom is bound is displaced upwards by 0.3 \AA with respect to the pristine surface configuration. The calculated magnetic moment for the spin of the Fe atom, considering an on-site Coulomb interactions $U = 5 \text{ eV}$, is $\mu_S \approx 4.36\mu_B$, with μ_B the Bohr magneton; this indicates a local spin $S = 2$. The DFT-calculated valence electron spin density (Fig. 1c) shows that the axial symmetry is largely intact. Thus, we can expect the orbital moment to be preserved in the out-of-plane direction, while it is quenched in-plane. The typical overestimation of the orbital momentum quenching by DFT calculations precludes a quantitative description of \mathbf{L} , and thus, of the resulting MAE [19, 20].

Instead, here we adopt an alternative strategy: we carry out an electronic multiplet calculation based on a point-charge model (PCM) description of the crystal field, where electron-electron repulsion between Fe d -electrons, spin-orbit coupling, and Zeeman contributions are considered explicitly [21, 22]. The atomic positions and charges are extracted from the DFT calculations (see Supplementary Material for additional information). A similar method was applied successfully to study the spin excitations of Fe on MgO [23].

Figure 2a shows the lowest energy levels as derived from the multiplet calculations. The crystal field (CF) contribution is separated into its axial and transverse components: the former preserves the 10-fold ground state degeneracy, while the latter splits this into two spin quintuplets. The spin-orbit coupling—where $\lambda_{SO} = -9.60 \text{ meV}$ for the PCM, and -9.41 meV for the spin-orbit model—partially lifts the degeneracy within the two quintuplets. Finally, the magnetic field B_z along the out-of-plane direction breaks all remaining degeneracies. At finite magnetic fields, the lowest two states have orbital moments $L_z = \pm 1.98$, closely approaching the free-atom value. Below, we will approximate these two states as $L_z = \pm 2$.

When interpreting spin excitation spectroscopy on individual magnetic atoms, it is convenient to employ an effective spin Hamiltonian [12, 24, 25]. However, in this situation the unquenched orbital moment makes the effective spin framework incomplete [26, 27]. Instead, we

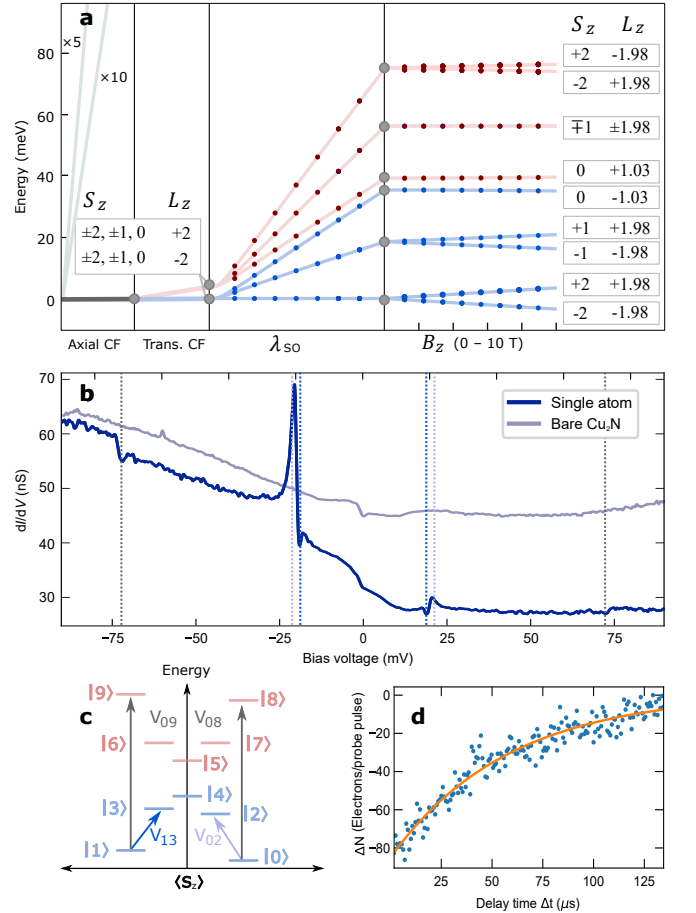


FIG. 2. (a) Multiplet calculations derived using both the PCM (solid lines) and the spin-orbit model (dots). The expectation values of S_z and L_z are indicated for each state. The transverse crystal field generates two distinct spin quintuplets (blue and red). The energy scale is defined relative to the ground state energy, except in the rightmost panel where the Zeeman splitting is considered, in which case the absolute energies are plotted. (b) Differential conductance (dI/dV) spectroscopy performed with a functionalized tip on a single Fe atom and on bare Cu_2N ($T = 0.5 \text{ K}$, $B_z = 4 \text{ T}$, $400 \mu\text{V}$ modulation, taken at -90 mV , 8 nA). Spin and orbital excitations are marked with blue and grey dotted lines, respectively. (c) Schematic representation of the two lowest quintuplets. The observed transitions are indicated with arrows, corresponding to the dotted lines in (b). (d) Pump-probe spectroscopy indicating a relaxation time of $T_1 = 58 \pm 4 \mu\text{s}$ at $B_z = 1 \text{ T}$, with pump and probe voltages of 150 mV and 14 mV , respectively, and a set-point of 500 pA , 30 mV .

use the following anisotropic spin-orbit Hamiltonian [27]

$$\hat{H} = B_2^0 \hat{O}_2^0 + B_4^0 \hat{O}_4^0 + B_4^4 \hat{O}_4^4 + \lambda_{SO} \hat{\mathbf{L}} \cdot \hat{\mathbf{S}} + \mu_B (\hat{\mathbf{L}} + 2\hat{\mathbf{S}}) \cdot \mathbf{B}, \quad (1)$$

where \hat{O}_k^q and B_k^q are the Stevens operators and their associated coefficients, respectively. The last term represents the Zeeman energy due to an external field \mathbf{B} . As we consider both the spin \mathbf{S} and orbital moment \mathbf{L} , there is no need to invoke the Landé g-factor. The results of

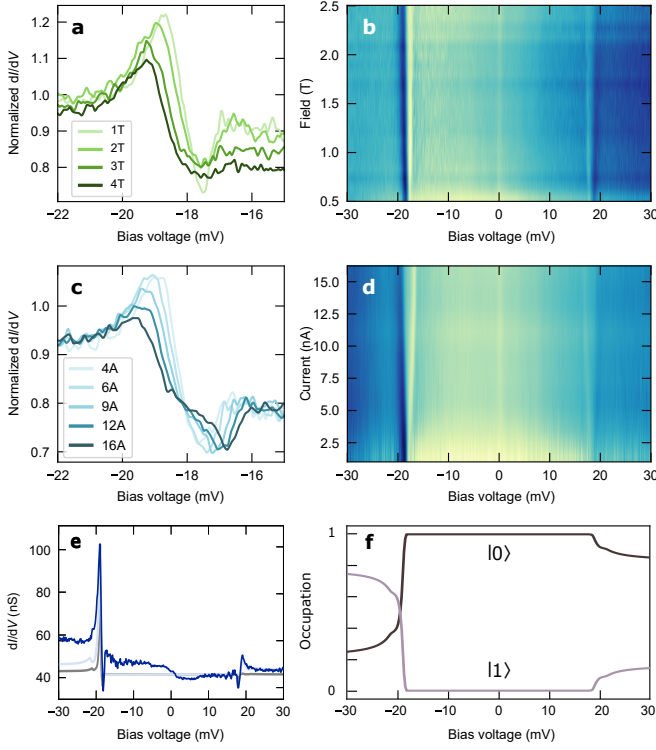


FIG. 3. (a) Differential conductance spectroscopy for different values of the external magnetic field. (b) Color map of dI/dV spectroscopy as a function of magnetic field. (c) Same as (a), but for different current set-points. (d) Same as (b), but as function of the current set-point. (e) Spectroscopy measurement (dark blue), compared to normalized transport calculations derived from the point-charge (grey) and spin-orbit (light blue) models. (f) Calculated voltage-dependent occupation of the two lowest energy states.

this model, implemented with optimal fitting parameters (see Supplementary Material), are depicted in Fig. 2a.

In Fig. 2b, we show an IETS measurement at a finite magnetic field, revealing a splitting of the zero-field excitation, with threshold voltages at 17.9 ± 0.2 meV and 19.4 ± 0.2 meV. These transitions can be probed with a tip that is functionalized by picking up individual Fe atoms from the surface. The results of Fig. 2a allow us to uniquely assign the observed transitions to excitations between specific states. The lower energy excitations are spin-only transitions ($\Delta S_z = \pm 1$, $\Delta L_z = 0$) corresponding to an excitation from the ground state $|S_z, L_z\rangle = |-2, -2\rangle \equiv |0\rangle$ to $|-1, -2\rangle \equiv |2\rangle$, corresponding to an excitation threshold voltage V_{02} , as well as from the $|+2, +2\rangle \equiv |1\rangle$ state to $|+1, +2\rangle \equiv |3\rangle$, with threshold V_{13} (Fig. 2c). At zero field, $|V_{02}| = |V_{13}| = 18.4 \pm 0.1$ meV.

We trace the evolution of the magnetic behavior of the single atom as a function of external field: in Fig. 3a and b, we show IETS measurements performed from 0.5 to 4 T. The measurements indicate a shift in the threshold voltage of 0.21 ± 0.02 meV/T. When expressed in terms of an effective $S = 2$ spin model in the absence of orbital

angular momentum [12], this shift would correspond to a Landé factor of ~ 3 , on par with previously reported large values [7, 8, 28].

In the absence of non-equilibrium effects, inelastic spin excitations, with $\Delta S_z = \pm 1$, are characterized by approximately square steps in the differential conductance [29], which originate from cotunneling events [30, 31]. However, additional nonlinearities may appear at the threshold voltage due to changes in the instantaneous spin state of the atom, which modify the magnetoresistance of the junction [14, 32]. The dynamical effects at the inelastic tunneling threshold voltage are indicative of relaxation times from state $|1\rangle$ longer than the average time between two tunneling electrons (~ 200 ps at 1 nA). We perform pump-probe spectroscopy (Fig. 2d) to find a relaxation time $T_1 = 58 \pm 4$ μ s.

As the presence of non-equilibrium features is attributed to dynamic processes linked to the inelastic electron transport, they are expected to be conductance-dependent. We investigate this dependence by performing dI/dV measurements as a function of current set-point, as shown in Fig. 3c and d. For this range of conductance values, we observe a decrease in the strength of the nonlinearity [32, 33] and a shift in the inelastic steps, due to the local field from the exchange interaction between the Fe atom and the tip [34].

Further insight can be obtained by simulating the non-equilibrium dynamics of the local spin (Fig. 3e). This is done on two fronts: on one hand, starting from the point-charge model calculation, we calculate the transition rates and the non-equilibrium occupations in the weak coupling limit using a co-tunneling description of transport [35, 36]. On the other, we use the spin-orbit model Eq. (1), where the evolution of the occupation is accounted for by a Pauli master equation [30, 31]. Tracing the occupation of the two lowest spin states as a function of voltage (Fig. 3f) delineates that below the inelastic threshold voltage, the ground state occupation exceeds 90%. Once the applied voltage reaches the excitation threshold, spin-flip excitations cause a significant drop in the occupation of $|0\rangle$. Due to the spin polarization of the tip ($\eta = 0.33$), spin-pumping is more favored for negative bias.

In addition, we consistently observe a higher energy excitation at 73.9 ± 0.4 meV (see Fig. 2b), which we denote by the threshold voltage V_{08} . This feature corresponds to an excitation from the ground state $|S_z, L_z\rangle = |-2, -2\rangle$ to the excited state $|-2, +2\rangle \equiv |8\rangle$; i.e., going from the lower spin quintuplet to the upper spin quintuplet (see Fig. 2c). Unlike a conventional spin excitation—in which the tunneling electron spin only interacts with the atom's spin ($|\Delta S_z| \leq 1$), leaving the orbital moment unchanged—we observe an independent excitation of only the orbital moment, with $\Delta L_z = 4$. Since the orbital moment of the magnetic atom is in this case preserved, it can be excited inelastically. Although or-

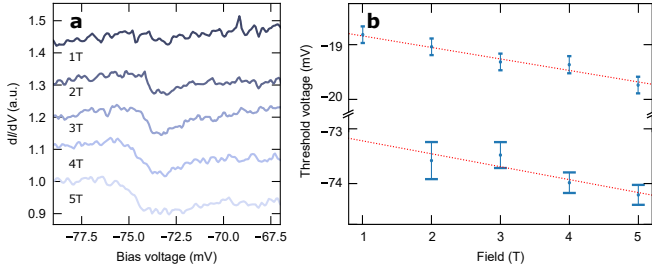


FIG. 4. (a) Differential conductance spectroscopy showing transitions at ~ 73 meV, for various magnetic fields (90 mV, 8 nA), normalized and shifted vertically (with respect to the 5 T spectrum) for clarity. Overlaid are the corresponding transport calculations (dotted lines) derived from the point charge model, horizontally shifted by -1.9 meV to match the experimentally derived threshold voltage. (b) The measured threshold voltages V_{02} and V_{08} as a function of the external magnetic field. Dashed lines are linear fits, indicating a shift of 0.21 ± 0.02 meV/T for the V_{02} transition and 0.24 ± 0.8 meV/T for the V_{08} transition.

orbital excitations have been previously reported [37, 38], this is the first instance of an independent rotation of an unquenched orbital moment. These transitions are not accounted for by the usual spin exchange terms $J\vec{S} \cdot \vec{\sigma}$ [30, 31].

Rather, this orbital transition can be understood via a co-tunneling path that takes into account both the spin and the orbital momentum of the initial, intermediate and final states [35, 36]. Since the transition is expected to occur with similar amplitude for the hole and electron charged states, we will focus on the latter for the following discussion. The dominant channel is mediated through the negatively charged intermediate state $|S_z = -3/2\rangle|L_z = 0\rangle$. As the orbital and spin matrix elements can be separated here, we choose to use product state notation in the description of the co-tunneling path. Accordingly, the co-tunneling transition amplitude between the ground state $|0\rangle$ and the excited state $|8\rangle$ can be understood by introducing the creation and annihilation operators, $\hat{d}_{\sigma_z \ell_z}^\dagger$ and $\hat{d}_{\sigma_z \ell_z}$, for an electron with spin σ_z in an orbital with angular momentum ℓ_z . The dominant transition amplitude between states $|0\rangle$ and $|8\rangle$ is thus proportional to [35, 36]

$$\langle +2 | \langle -2 | \hat{d}_{\frac{1}{2}, -2}^\dagger | -3/2 \rangle | 0 \rangle \langle 0 | \langle -3/2 | \hat{d}_{\frac{1}{2}, +2}^\dagger | -2 \rangle | -2 \rangle. \quad (2)$$

This cotunneling path corresponds to a spin-up electron tunneling onto the $\ell_z = +2$ orbital, thus creating a charged virtual state with a net spin $S_z = -3/2$ and orbital moment $L_z = 0$. An electron then tunnels off the $\ell_z = -2$ orbital, restoring the net spin to $S_z = -2$ and changing the orbital moment to $L_z = +2$, thereby completing the $\Delta S_z = 0, \Delta L_z = 4$ transition.

We expect this excitation to correspond to two transitions: one from $|0\rangle$ to $|8\rangle$, and another from $|1\rangle$ to $|9\rangle$, which should respectively split as a function of magnetic

field due to the Zeeman effect. Accordingly, we trace the evolution of this transition from 1 to 5 T (Fig. 4a): we observe that the step is broadened as the field is increased, which is compatible with a splitting of V_{08} and V_{19} . This behaviour is well reproduced by the transport calculations derived from the point-charge model. In fact, the high degree of agreement here is remarkable, as the point-charge calculations are based solely on DFT results, and thereby don't have any additional fitting parameters. However, it is worth noting that the threshold voltage corresponding to the orbital excitation is off by ~ 2 meV when comparing the transport calculations to the experimental data. In order to properly compare the evolution of the step, we correct for this shift in Fig. 2a.

While the orbital transition does not exhibit the same nonlinearities characteristic of the lower energy spin excitations at ~ 18 meV, it does shift with field, specifically at a rate of 0.24 ± 0.8 meV/T (see Fig. 2b). By comparison, the shift predicted by the multiplet calculation is 0.23 meV/T.

In this work we studied the magnetic properties of individual Fe atoms bound to N-sites on the Cu_2N lattice, which exhibit large magnetic anisotropy, evidenced by an 18 meV spin excitation at zero field, resulting from an unquenched orbital moment $L = 1.98$. Spectroscopy measurements reveal that the inelastic spin transition exhibits a large shift with both magnetic field and current set-point. We observe an additional transition at 73 meV, which we identify as a $\Delta L_z = 4$ rotation of the orbital moment. We rationalize these experimental results in terms of both a multiplet electronic calculation and an effective anisotropic spin-orbit Hamiltonian. As Fe atoms bound on N-sites are easily manipulable, these results form a promising basis for future research on extended spin lattices.

The authors thank the Netherlands Organisation for Scientific Research (NWO) and the European Research Council (ERC Starting Grant 676895 'SPINCAD'). FD acknowledges financial support from Basque Government, grant IT986-16 and Canary Islands program *Viera y Clavijo* (Ref. 2017/0000231). All data presented in this work is publicly available with identifier 10.5281/zenodo.3466636.

* r.rejali@tudelft.nl

† a.f.otte@tudelft.nl

- [1] S. Loth, S. Baumann, C. P. Lutz, D. M. Eigler, and A. J. Heinrich, *Science* **335**, 196 (2012).
- [2] A. Khajetoorians, J. Wiebe, B. Chilian, and R. Wiesendanger, *Science* **332**, 1062 (2011).
- [3] F. D. Natterer, K. Yang, W. Paul, P. Willke, T. Choi, T. Greber, A. J. Heinrich, and C. P. Lutz, *Nature* **543**, 226 (2017).
- [4] F. Donati, S. Rusponi, S. Stepanow, C. Wackerlin,

- A. Singha, L. Persichetti, R. Baltic, K. Diller, F. Patthey, E. Fernandes, J. Dreiser, Ž. Šljivančanin, K. Kummer, C. Nistor, P. Gambardella, and H. Brune, *Science* **352**, 318 (2016).
- [5] D. I. Khomskii, *Transition Metal Compounds* (Cambridge University Press, 2014).
- [6] O. Eriksson, B. Johansson, R. C. Albers, A. M. Boring, and M. S. S. Brooks, *Phys. Rev. B* **42**, 2707 (1990).
- [7] S. Baumann, F. Donati, S. Stepanow, S. Rusponi, W. Paul, S. Gangopadhyay, I. G. Rau, G. E. Pacchioni, L. Gragnaniello, M. Pivetta, J. Dreiser, C. Piamonteze, C. P. Lutz, R. M. Macfarlane, B. A. Jones, P. Gambardella, A. J. Heinrich, and H. Brune, *Phys. Rev. Lett.* **115**, 237202 (2015).
- [8] I. G. Rau, S. Baumann, S. Rusponi, F. Donati, S. Stepanow, L. Gragnaniello, J. Dreiser, C. Piamonteze, F. Nolting, S. Gangopadhyay, O. R. Albertini, R. M. Macfarlane, C. P. Lutz, B. A. Jones, P. Gambardella, A. J. Heinrich, and H. Brune, *Science* **344**, 988 (2014).
- [9] I. Gallardo, A. Arnau, F. Delgado, R. Baltic, A. Singha, F. Donati, C. Wckerlin, J. Dreiser, S. Rusponi, and H. Brune, *New Journal of Physics* **21**, 073053 (2019).
- [10] T. Choi and J. A. Gupta, *Journal of Physics: Condensed Matter* **26**, 394009 (2014).
- [11] C. F. Hirjibehedin, C. P. Lutz, and A. J. Heinrich, *Science* **312**, 1021 (2006).
- [12] C. F. Hirjibehedin, C.-Y. Lin, A. F. Otte, M. Ternes, C. P. Lutz, B. A. Jones, and A. J. Heinrich, *Science* **317**, 1199 (2007).
- [13] A. F. Otte, M. Ternes, K. von Bergmann, S. Loth, H. Brune, C. P. Lutz, C. F. Hirjibehedin, and A. J. Heinrich, *Nature Physics* **4**, 847 EP (2008).
- [14] S. Loth, K. von Bergmann, M. Ternes, A. F. Otte, C. P. Lutz, and A. J. Heinrich, *Nature Physics* **6**, 340 EP (2010).
- [15] B. Bryant, A. Spinelli, J. J. T. Wagenaar, M. Gerrits, and A. F. Otte, *Phys. Rev. Lett.* **111**, 127203 (2013).
- [16] A. Spinelli, B. Bryant, F. Delgado, J. Fernández-Rossier, and A. F. Otte, *Nature Materials* **13**, 782 (2014).
- [17] A. Spinelli, M. P. Rebergen, , and A. F. Otte, *Journal of Physics: Condensed Matter* **27**, 243203 (2015).
- [18] J. Gobeil, D. Coffey, S.-J. Wang, and A. F. Otte, *Surface Science* **679**, 202 (2019).
- [19] P. Błoński, A. Lehnert, S. Dennler, S. Rusponi, M. Etzkorn, G. Moulas, P. Bencok, P. Gambardella, H. Brune, and J. Hafner, *Phys. Rev. B* **81**, 104426 (2010).
- [20] L. Peters, I. Di Marco, O. Grånäs, E. Şaşıoğlu, A. Altun, S. Rossen, C. Friedrich, S. Blügel, M. I. Katsnelson, A. Kirilyuk, and O. Eriksson, *Phys. Rev. B* **93**, 224428 (2016).
- [21] A. Ferrón, F. Delgado, and J. Fernández-Rossier, *New J. Phys.* **17**, 033020 (2015).
- [22] J. L. Lado, A. Ferrón, and J. Fernández-Rossier, *Phys. Rev. B* **96**, 205420 (2017).
- [23] S. Baumann, *Investigation of the unusual magnetic properties of Fe and Co on MgO with high spatial, energy and temporal resolution*, Ph.D. thesis, University_of_Basel (2015).
- [24] F. Donati, Q. Dubout, G. Autès, F. Patthey, F. Calleja, P. Gambardella, O. V. Yazyev, and H. Brune, *Phys. Rev. Lett.* **111**, 236801 (2013).
- [25] A. F. Otte, M. Ternes, K. von Bergmann, S. Loth, H. Brune, C. P. Lutz, C. F. Hirjibehedin, and A. J. Heinrich, *Nature Physics* **4**, 847 EP (2008).
- [26] T. Schuh, T. Balashov, T. Miyamachi, S.-Y. Wu, C.-C. Kuo, A. Ernst, J. Henk, and W. Wulfhekel, *Phys. Rev. B* **84** (2011), 10.1103/PhysRevB.84.104401.
- [27] A. Abragam and B. Bleaney, *Electron Paramagnetic Resonance of Transition Ions* (Oxford University Press, Oxford, 1970).
- [28] B. Chilian, A. A. Khajetoorians, S. Lounis, A. T. Costa, D. L. Mills, J. Wiebe, and R. Wiesendanger, *Phys. Rev. B* **84**, 212401 (2011).
- [29] M. Ternes, *New Journal of Physics* **17**, 063016 (2015).
- [30] M. Ternes, *Progress in Surface Science* **92**, 83 (2017).
- [31] F. Delgado and J. Fernández-Rossier, *Progress in Surface Science* **92**, 40 (2017).
- [32] S. Rolf-Pissarczyk, S. Yan, L. Malavolti, J. A. J. Burgess, G. McMurtrie, and S. Loth, *Phys. Rev. Lett.* **119**, 217201 (2017).
- [33] M. Grundmann, *The Physics of Semiconductors* (Springer-Verlag, 2006).
- [34] S. Yan, D.-J. Choi, J. A. J. Burgess, S. Rolf-Pissarczyk, and S. Loth, *Nature Nanotechnology* **10**, 40 EP (2014).
- [35] F. Delgado and J. Fernández-Rossier, *Phys. Rev. B* **84**, 045439 (2011).
- [36] J. Reina Gálvez, C. Wolf, F. Delgado, and N. Lorente, *Phys. Rev. B* **100**, 035411 (2019).
- [37] B. Bryant, R. Toskovic, A. Ferrón, J. Lado, A. Spinelli, J. Fernández-Rossier, and A. F. Otte, *Nano Letters*, **15**, 6542 (2015).
- [38] B. Kiraly, A. N. Rudenko, W. M. van Weerdenburg, D. Wegner, M. I. Katsnelson, and A. A. Khajetoorians, *Nature communications* **9**, 3904 (2018).